

# Global analysis of proton elastic form factor data with two-photon exchange corrections

J. Arrington

*Argonne National Laboratory, Argonne, Illinois 60439, USA*

W. Melnitchouk

*Jefferson Lab, Newport News, Virginia 23606, USA*

J. A. Tjon

*Physics Department, University of Utrecht, The Netherlands*

(Dated: October 31, 2018)

We use the world's data on elastic electron-proton scattering and calculations of two-photon exchange effects to extract corrected values of the proton's electric and magnetic form factors over the full  $Q^2$  range of the existing data. Our analysis combines the corrected Rosenbluth cross section and polarization transfer data, and is the first extraction of  $G_E$  and  $G_M$  including explicit two-photon exchange corrections and their associated uncertainties. In addition, we examine the angular dependence of the corrected cross sections, and discuss the possible nonlinearities of the cross section as a function of  $\epsilon$ .

PACS numbers: 25.30.Bf, 13.40.Gp, 14.20.Dh

## I. INTRODUCTION

As one of the most fundamental observables which characterize the composite nature of the nucleon, electromagnetic form factors have over the past few decades provided considerable insight into the nucleon's internal structure [1, 2, 3, 4]. In the commonly used one-photon exchange approximation to electron-nucleon scattering, the form factors depend only on the four-momentum transfer squared,  $-Q^2$ . At low  $Q^2$  the Fourier transforms of the form factors give information on the charge and magnetization distributions of the nucleon.

The expectation from perturbative QCD is that the  $Q^2$  dependence of the Sachs electric,  $G_E(Q^2)$ , and magnetic,  $G_M(Q^2)$ , form factors should be the same at large  $Q^2$ , and early data indeed suggested approximate scaling of the ratio  $G_E/G_M$  with  $Q^2$  [5]. These data were analyzed using the Rosenbluth or longitudinal-transverse (LT) separation technique, in which the form factor ratio is extracted by examining the elastic cross section as a function of the scattering angle,  $\theta$ . The cross section at  $\theta = 180^\circ$  depends only on the magnetic form factor, while the cross section at smaller angles is a combination of magnetic and electric contributions. At large  $Q^2$ , the contribution from the electric form factors is small, and here the technique has reduced sensitivity to  $G_E$ .

Recent experiments at Jefferson Lab [6, 7, 8], utilizing the polarization transfer (PT) technique to measure the ratio  $G_E/G_M$ , found the surprising result that  $G_E$  decreases more rapidly than  $G_M$  at large  $Q^2$ . This indicates a substantially different spatial distribution of the charge and magnetization of the nucleon [9], raising questions as to the impact of angular momentum and relativistic effects on the nucleon structure [10, 11, 12, 13, 14, 15, 16]. The virtue of the PT technique is that it is sensitive only to the ratio  $G_E/G_M$ , rather than the sum of a large mag-

netic and small electric contribution, and so does not suffer from the dramatically reduced sensitivity to  $G_E$  of the LT separation at large  $Q^2$ . However, the two techniques disagree significantly even in the region where they both yield precise results [17], and a puzzle has existed about the origin of the discrepancy.

An accurate determination of the proton electric and magnetic form factors is also important as these impact on our knowledge of other quantities whose extraction is sensitive to  $G_E$  and  $G_M$ . In some cases, uncertainties in the proton form factors will be magnified, yielding even larger corrections in other observables.

A number of recent theoretical studies of two-photon exchange (TPE) in elastic  $ep$  scattering have been performed [18, 19, 20, 21, 22, 23, 24, 25] (see also Ref. [26] for a recent review). These indicate that TPE effects give rise to a strong angular-dependent correction to the elastic cross section, which can lead to large corrections to the LT-extracted  $G_E/G_M$  ratio. In fact, the results of quantitative calculations based both on hadronic intermediate states [22, 23, 24, 25, 27] and on generalized parton distributions [20, 21], provide strong evidence that TPE effects can account for most of the difference between the LT and PT data sets.

While the TPE analyses are very suggestive of the resolution of the problem, there exists some residual discrepancy between the TPE-corrected data sets. Moreover, the effects of the TPE correction on the extraction of  $G_E$  and  $G_M$  have in practice been estimated using a linear approximation to the correction over an arbitrary angular range [19, 22], which can yield significant uncertainties in evaluating the effect of TPE on the form factor extractions, especially at high  $Q^2$ . An accurate determination of  $G_E$  and  $G_M$  requires analyzing the elastic scattering data taking into account the TPE effects *directly* on the cross sections. This is the primary aim of the present

paper.

Our approach will be to apply the TPE corrections directly to the cross section data, estimate the uncertainties in the TPE corrections, and compare TPE-corrected results to polarization measurements. We then use the corrected cross section results, combined with polarization transfer measurements, to extract the best possible values and uncertainties for  $G_E$  and  $G_M$  of the proton.

The outline of this paper is as follows. In Sec. II we review the formalism of elastic  $ep$  scattering in the presence of TPE effects and discuss the TPE corrections which we apply to the data. We also study the effect of TPE on the ratio of electron–proton to positron–proton elastic cross sections. In Sec. III, TPE corrections are applied to the cross section and polarization transfer measurements, and a combined analysis of all measurements is performed. We provide parameterizations of the corrected form factors, as well as a direct fit to the elastic cross section, without correction for TPE effects. Finally, in Sec. IV we summarize our results and discuss future work.

## II. ELASTIC $ep$ SCATTERING

### A. Born approximation

In the one-photon exchange or Born approximation the differential cross section is given in terms of the Born amplitude  $\mathcal{M}_0$  by:

$$\frac{d\sigma_0}{d\Omega} = \left( \frac{\alpha}{4MQ^2} \frac{E'}{E} \right)^2 |\mathcal{M}_0|^2 = \sigma_{\text{Mott}} \frac{1}{\varepsilon(1+\tau)} \sigma_R, \quad (1)$$

where  $\sigma_{\text{Mott}}$  is the cross section for scattering on a point particle,  $E$  and  $E'$  are initial and final electron energies, respectively,  $\tau = Q^2/4M^2$ , and  $\alpha = e^2/4\pi$  is the electromagnetic fine structure constant. In performing a Rosenbluth separation, it is convenient to work with the reduced cross section,  $\sigma_R$ :

$$\sigma_R = \tau G_M^2(Q^2) + \varepsilon G_E^2(Q^2), \quad (2)$$

where  $\varepsilon = [1 + 2(1 + \tau) \tan^2(\theta/2)]^{-1}$  is the virtual photon polarization parameter. This decomposition allows a direct separation of  $G_E$  and  $G_M$  from the  $\varepsilon$  dependence of  $\sigma_R$ . In the Born approximation the form factors are functions of only a single variable,  $Q^2$ . Effects beyond one-photon exchange introduce additional  $\varepsilon$  dependence.

The polarization transfer method involves the scattering of a polarized electron beam from an unpolarized target, with measurement of the polarization of the recoiling proton. In the Born approximation the ratio of the transverse to longitudinal recoil polarizations yields [28]:

$$R = \mu_p \frac{G_E}{G_M} = -\mu_p \sqrt{\frac{\tau(1+\varepsilon)}{2\varepsilon}} \frac{P_T}{P_L}, \quad (3)$$

where  $\mu_p$  is the proton magnetic moment, and  $P_T$  ( $P_L$ ) is the polarization of the recoil proton transverse (longitudinal) to the proton momentum in the scattering plane. It should be noted that both  $P_T$  and  $P_L$  individually depend only on the ratio  $G_E/G_M$ , with  $P_T$  ( $P_L$ ) being strongly (weakly) dependent on  $G_E/G_M$ . In most experiments, however, the ratio of the two polarization components is used, with  $P_T$  providing sensitivity to the form factor ratio, and the ratio to  $P_L$  yielding a result that is independent of the overall beam and target polarization and/or analyzing power of the detector. One has similar sensitivity to  $G_E/G_M$  in measurements of the beam-target asymmetry [29, 30, 31].

### B. TPE: Unpolarized $ep$ scattering

With the inclusion of radiative corrections to order  $\alpha$ , the elastic scattering cross section in Eq. (1) is modified according to:

$$\frac{d\sigma_0}{d\Omega} \rightarrow \frac{d\sigma}{d\Omega} = \frac{d\sigma_0}{d\Omega} (1 + \delta_{\text{RC}}), \quad (4)$$

where  $\delta_{\text{RC}}$  represents one-loop corrections, including vacuum polarization, electron and proton vertex, and two-photon exchange corrections, in addition to inelastic bremsstrahlung for real photon emission [32].

As discussed in Refs. [19, 22], the amplitude for the one-loop virtual corrections,  $\mathcal{M}_1$ , can be written as the sum of a factorizable term, proportional to the Born amplitude  $\mathcal{M}_0$ , and a non-factorizable component,  $\overline{\mathcal{M}}_1$ :

$$\mathcal{M}_1 = f(Q^2, \varepsilon) \mathcal{M}_0 + \overline{\mathcal{M}}_1. \quad (5)$$

The ratio of the full,  $\mathcal{O}(\alpha)$  cross section to the Born cross section can then be written as:

$$1 + \delta_{\text{RC}} = \frac{|\mathcal{M}_0 + \mathcal{M}_1|^2}{|\mathcal{M}_0|^2}, \quad (6)$$

with the correction  $\delta_{\text{RC}}$  given by:

$$\delta_{\text{RC}} = 2f(Q^2, \varepsilon) + \frac{2\Re\{\mathcal{M}_0^\dagger \overline{\mathcal{M}}_1\}}{|\mathcal{M}_0|^2}. \quad (7)$$

The contributions to the functions  $f(Q^2, \varepsilon)$  from the electron vertex, vacuum polarization, and proton vertex terms depend only on  $Q^2$ , and hence do not affect the LT separation, aside from an overall normalization factor. Of the factorizable terms, only the IR-divergent TPE correction contributes to the  $\varepsilon$  dependence of the virtual photon corrections [19].

The non-factorizable terms contained in  $\overline{\mathcal{M}}_1$  arise from the finite nucleon vertex and TPE corrections, which depend explicitly on nucleon structure. For the proton vertex correction, the  $\varepsilon$  dependence is weak, and will not significantly affect the LT analysis [33]. For the inelastic bremsstrahlung cross section, the amplitude for real photon emission can also be written in the form of Eq. (5).

In the soft photon approximation, in which one of the two exchanged photons is taken to be on-shell, the complete amplitude is completely factorizable. A significant  $\varepsilon$  dependence arises due to the frame dependence of the angular distribution of the emitted photon. These corrections, together with external bremsstrahlung, contain the main  $\varepsilon$  dependence of the radiative corrections, and are accounted for in standard experimental analyses. They are generally well understood, and in fact enter differently depending on whether the electron or proton are detected in the final state [34, 35].

The only remaining term at  $\mathcal{O}(\alpha)$  that can introduce a non-negligible  $\varepsilon$  dependence, namely the non-factorizable part of the TPE contribution, is typically not accounted for in cross section extractions. The total TPE amplitude,  $\mathcal{M}_{2\gamma}$ , can be written as:

$$\delta_{2\gamma} = \frac{2\Re\{\mathcal{M}_0^\dagger \mathcal{M}_{2\gamma}\}}{|\mathcal{M}_0|^2}, \quad (8)$$

where in principle the TPE amplitude  $\mathcal{M}_{2\gamma}$  includes all possible (off-shell) hadronic intermediate states.

In typical experimental analyses of electromagnetic form factor data, radiative corrections are implemented using a formalism based on the Mo & Tsai (MT) prescription [32, 36]. While the detailed implementation has been improved over the years [5, 37], the treatment of TPE has remained unchanged from the original work. The TPE effects are partially included in the MT approach by approximating the TPE amplitude by its infrared (IR) divergent part.

A more detailed examination of the loop integrals [33] yields the same IR-divergent contribution as Mo & Tsai [32],  $\delta_{\text{IR}}(\text{MT})$ , but also yields an IR-finite contribution. The IR-finite part, which is usually neglected in the standard data analyses, was found in Refs. [19, 22] to have a significant  $\varepsilon$  dependence, and is explicitly included here. To isolate the effect of the additional TPE contributions on the data, Blunden et al. [19, 22] consider the difference:

$$\Delta \equiv \delta_{2\gamma} - \delta_{\text{IR}}(\text{MT}), \quad (9)$$

in which the IR divergences cancel. We will follow this approach and therefore reference the  $\varepsilon$  dependence of the full calculation of  $\delta_{2\gamma}$  with that of  $\delta_{\text{IR}}(\text{MT})$ .

The results for the difference,  $\Delta(\varepsilon, Q^2)$ , between the full calculation and the MT approximation are most significant at low  $\varepsilon$ , and essentially vanish at large  $\varepsilon$ . At the lower  $Q^2$  values,  $\Delta$  is approximately linear in  $\varepsilon$ , but significant deviations from linearity are observed with increasing  $Q^2$ , especially at smaller  $\varepsilon$  [22].

The effect of TPE on the LT extractions of  $G_E$  is greatest at large  $Q^2$  since because the cross section here is not very sensitive to  $G_E$ . However, the TPE corrections to the cross section have a relatively weak  $Q^2$  dependence, and are therefore still significant at low  $Q^2$  values, where many high-precision measurements of nucleon or nuclear

structure are performed that require accurate knowledge of the proton form factors.

### C. TPE: Theoretical uncertainty

For the dominant nucleon elastic TPE contribution, the main uncertainty arises from the input form factors at the internal  $\gamma^*NN$  vertices in the loop diagrams. Because the intermediate state nucleon is off-shell, in principle the “half off-shell” form factors here need not be the same as the free nucleon form factors, and can explicitly depend on the intermediate nucleon four-momentum. The off-shell dependence is of course unknown, but in practice it is sufficient, at least at low  $Q^2$ , to approximate these by the free form factors.

For the calculation in Ref. [22] it was necessary for technical reasons to parameterize the internal form factors by sums of monopole functions, which were fitted to realistic parameterizations of form factor data. In the actual analysis [22] the form factor parameterization was taken from the global fit in Ref. [38]. For comparison, more recent fits to data [39, 40] were also used, and the sensitivity of the TPE correction  $\Delta(\varepsilon, Q^2)$  to the particular form was found to be negligible up to  $Q^2 \sim 10 \text{ GeV}^2$ .

In the present analysis we use the more recent global form factor parameterization from Ref. [39] with  $G_E$  constrained by the PT data. A three-monopole fit to this parameterization provides a very good fit for  $G_E$  and  $G_M$  over the range where both the form factors are constrained by data. Above  $Q^2 = 6 \text{ GeV}^2$ , the three-monopole fit to  $G_E$  becomes unconstrained, leading to unstable results for the TPE corrections. Here we instead use a dipole approximation for the form factors, which guarantees a smooth extrapolation to high  $Q^2$ , and matches onto the asymptotic high- $Q^2$  behavior expected from perturbative QCD. The difference between the TPE results at  $Q^2 = 6 \text{ GeV}^2$  with the “realistic” and dipole form factors is not significant, which is consistent with the findings in Ref. [22].

Estimates of the contributions to  $\Delta(\varepsilon, Q^2)$  from higher-mass intermediate states have been made by a number of authors [23, 27, 41, 42, 43, 44]. In a recent analysis, Kondratyuk et al. [23] evaluated the contribution of the  $\Delta(1232)$  resonance, which is known to play an important role in hadronic structure, between  $Q^2 = 1$  and  $6 \text{ GeV}^2$ . The  $\Delta(1232)$  intermediate state contribution was found to be smaller in magnitude than the nucleon contribution, with an opposite sign at backward scattering angles where the TPE effects are largest. For realistic choices of the  $\gamma N\Delta$  vertex, and couplings obtained from a hadronic model analysis of Compton scattering off the nucleon [45], the magnitude of the  $\Delta(1232)$  contribution was found to be around 1/4 of that of the nucleon at low and intermediate  $Q^2$ . The  $\Delta(1232)$  therefore tends to cancel some of the TPE effect from the nucleon elastic intermediate state, modifying the cross section by between  $-1\%$  and  $2\%$ . At larger  $Q^2$  the magnitude of the

$\Delta(1232)$  contribution increases, along with that of the nucleon elastic, although above  $Q^2 \sim 10 \text{ GeV}^2$  the reliability of the calculation is more questionable.

Effects of higher mass, spin- and isospin-1/2 and 3/2 resonances were also estimated recently by Kondratyuk & Blunden [27]. The excited states included in that analysis were the  $P_{11} N(1440)$  Roper resonance, the  $D_{13} N(1520)$ , and the odd-parity  $S_{11} N(1535)$  for isospin-1/2, and the  $S_{31} \Delta(1620)$  and  $D_{33} \Delta(1700)$  isospin-3/2 resonances. The photocouplings for these states were taken from the model [45] of nucleon Compton scattering at energies up to the first and second resonance regions, and a universal dipole form factor was applied for each of the  $\gamma N \rightarrow$  resonance transitions. In addition, the assumption was made that the transitions are mostly magnetic, with the electric being much smaller, and the Coulomb couplings are taken to be zero.

The overall scale of the higher mass contributions is approximately an order of magnitude smaller than the nucleon and  $\Delta(1232)$  for  $Q^2 \lesssim 6 \text{ GeV}^2$ . Moreover, these alternate in sign, with the  $P_{11}$ ,  $D_{13}$  and  $D_{33}$  contributions being mostly negative (as the nucleon), while the  $S_{11}$  and  $S_{31}$  mostly positive. For larger  $Q^2$  this model, as with all models based on hadronic degrees of freedom, is unlikely to be reliable.

Clearly the inclusion of the higher mass hadronic intermediate states is considerably more model dependent than the nucleon elastic or even the  $\Delta(1232)$  contribution, in view of uncertainties in the various photocouplings, the transition form factors, and the efficacy of representing high energy off-shell nucleon excitations by states of zero width. Effects of overlapping resonances, as well as the multihadron continuum, or non-resonant background, are expected to be increasingly important at larger  $Q^2$ . One could in principle constrain the high mass spectrum phenomenologically by Compton scattering data at high  $Q^2$ . Unfortunately these are not yet available, and one must rely on theoretical guidance.

From the point of view of quark-hadron duality, one expects that at large  $Q^2$  the intermediate state spectrum can be saturated either by including a large set of hadronic resonances, or by summing over quark degrees of freedom [46]. Although the approaches are in principle complementary, if  $Q^2$  is large enough a quark level calculation may provide a more efficient description. Such calculations have been performed in the context of generalized parton distributions (GPDs) [20, 21] within the “handbag” approximation, in which the scattering of the virtual photon takes place off a single quark in the proton. This should be the dominant (leading twist) contribution at high  $Q^2$ , although at intermediate  $Q^2$ , processes where the virtual photon interacts with different quarks in the proton (higher twist) are still important.

One of the uncertainties in the calculation is the choice of GPD, and in Ref. [21] a Gaussian valence ansatz is used. The calculation has a small but noticeable difference when using their modified Regge GPD, and has a similar dependence on the assumed quark mass. In ad-

dition, for the leading twist approximation to be applicable, both  $Q^2$  and the invariant mass squared  $s$  of the intermediate state are required to be large. In practice the constraint  $Q^2, s > M^2$  is used, which restricts the kinematic reach of the calculation to moderate and large  $\varepsilon$ . For  $Q^2 \sim 2 - 6 \text{ GeV}^2$ , one is restricted to  $\varepsilon > 0.2 - 0.4$ . The results show significant  $\varepsilon$  dependence with clear deviations from linearity at intermediate and large  $\varepsilon$ , and a weak  $Q^2$  dependence. The overall trend of the  $\varepsilon$  dependence is similar to that in Ref. [22], but smaller in magnitude. At high  $Q^2$  there appears little  $\varepsilon$  dependence for  $\varepsilon > 0.5$ , which yields little modification to the LT extraction of  $G_E/G_M$  dominated by data at large  $\varepsilon$ . At the highest  $Q^2$  points the partonic contribution explains about 1/2 of the discrepancy between the LT and PT results.

The indications from both the hadronic and partonic higher mass calculations are therefore that there is an additional effect at the level of a few percent on top of the nucleon elastic contribution, albeit with a sizable theoretical uncertainty. Given the difficulty in obtaining a reliable quantitative estimate of the higher mass contributions to TPE at high  $Q^2$ , rather than rely on a specific model, we take a more phenomenological approach.

At low  $Q^2$ , the correction is approximately linear with  $\varepsilon$ . While the calculations suggest increasing nonlinearities, they differ in the detailed  $\varepsilon$  dependence, and the data are consistent with very small nonlinearities [47]. We assume therefore a linear  $\varepsilon$  dependence for the form of the extra TPE correction. We make an estimate of the  $Q^2$  dependence of the additional terms from the calculations of the higher resonance states [27] and the GPD-based model [21], and apply this as the additional TPE correction. For  $Q^2 < 1 \text{ GeV}^2$ , we do not apply any additional TPE effect, as all indications are that it is very small. For  $Q^2 > 1 \text{ GeV}^2$ , we take a  $Q^2$  dependence that grows slowly with  $Q^2$ :

$$\delta_{2\gamma}^* = 0.01 [\varepsilon - 1] \frac{\ln Q^2}{\ln 2.2} \quad (Q^2 > 1 \text{ GeV}^2), \quad (10)$$

with  $Q^2$  in  $\text{GeV}^2$ , and apply a 100% uncertainty. This yields a correction linear in  $\varepsilon$  that decreases the  $\varepsilon = 0$  cross section by 1% at  $Q^2 = 2.2 \text{ GeV}^2$ , by 2% at  $4.8 \text{ GeV}^2$ , and by 3% at  $10.6 \text{ GeV}^2$ . This correction is then added to the calculated  $\delta_{2\gamma}$ .

As a further check, we compare the extraction of  $G_E/G_M$  from the TPE-corrected cross section data and the polarization transfer measurements, which is discussed in Sec. IIIB and shown in the bottom panel of Fig. 2, below. The additional correction brings the high- $Q^2$  LT  $G_E/G_M$  points into good agreement with the PT data, although the error on the corrected LT data is considerably larger at high  $Q^2$ .

While the effect of the TPE corrections on  $G_M$  is smaller, it can potentially have a large impact on global fitting. For instance, the TPE corrections for  $G_E$  shift around 10 – 15 data points by  $1 - 2\sigma$ , but for  $G_M$  there are of order 30 – 40 points affected by a  $2 - 3\sigma$  shift.

In addition, even though the TPE corrections to  $G_M$  are less dramatic than those for  $G_E$ , the uncertainties in the TPE effects when extracting  $G_M$  at large  $Q^2$  will still be important.

#### D. TPE: $e^-p$ vs. $e^+p$

While TPE corrections modify the unpolarized cross section, it is difficult to isolate TPE corrections from the Born cross section experimentally without independent knowledge of the proton form factors. Only deviations from the linear  $\varepsilon$  dependence predicted by Eq. (2) can be observed, and in practice these are found to be very small [47]. However, *direct* experimental evidence for the contribution of TPE can be obtained by examining the ratio of  $e^+p$  and  $e^-p$  cross sections. The Born amplitude changes sign under the interchange  $e^- \leftrightarrow e^+$ , while the TPE amplitude does not. The interference therefore has the opposite sign for electron and positron scattering, which will show up in the experimental ratio  $R^{e^+e^-} = \sigma_{e^+p}/\sigma_{e^-p} \approx (1 - 2\Delta)$ , where  $\Delta$  is defined in Eq. (9). Interference between electron and proton bremsstrahlung also yields a small difference, but this is corrected for in the extraction of  $R^{e^+e^-}$ .

Although the current data on elastic  $e^-p$  and  $e^+p$  scattering are sparse, there are some experimental constraints from early data taken at SLAC [48, 49], Cornell [50], DESY [51] and Orsay [52] (see also Ref. [53] and references therein). The data are predominantly at low  $Q^2$  and at forward scattering angles, corresponding to large  $\varepsilon$  ( $\varepsilon \gtrsim 0.7$ ), where the calculated  $2\gamma$  exchange contribution is small ( $\lesssim 1\%$ ). Nevertheless, the overall trend in the data reveals a small enhancement in  $R^{e^+e^-}$  at the lower  $\varepsilon$  values [53].

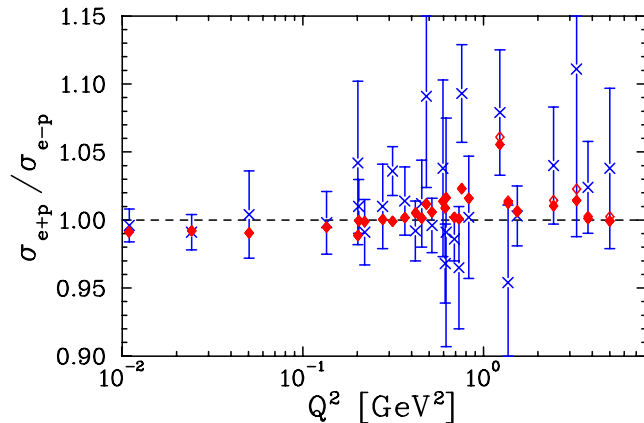


FIG. 1: Ratio of elastic  $e^+p$  to  $e^-p$  cross sections. The data (crosses) are taken from Ref. [53] and references therein. The filled diamonds show the ratio using the TPE calculation of Ref. [22], while the open diamonds include the additional contribution in Eq. (10), which modifies the high- $Q^2$  correction at low  $\varepsilon$ .

Figure 1 shows the extracted ratio,  $R^{e^+e^-}$ , compared

with the calculation of Ref. [22] (filled diamonds), and with the additional high mass contribution in Eq. (10) (open diamonds). The calculation is in good agreement with the data, although the errors on the data points are quite large. Clearly better quality data at backward angles and moderate  $Q^2$ , where an enhancement of up to  $\sim 10\%$  is predicted, would be needed for a more definitive test of the TPE mechanism. There is a planned experiment to perform a precise ( $\sim 1\%$ ) comparison of  $e^-p$  and  $e^+p$  scattering at  $Q^2 = 1.6 \text{ GeV}^2$  and  $\varepsilon \approx 0.4$  at the VEPP-3 storage ring [54]. An experiment to provide broader  $\varepsilon$  and  $Q^2$  coverage [55] at Jefferson Lab is approved to make such measurements up to  $Q^2 = 2 - 3 \text{ GeV}^2$  using a beam of  $e^+e^-$  pairs produced from a secondary photon beam.

#### E. TPE: Polarization observables

Naively, one expects the corrections to the spin-dependent cross sections to be of the same order of magnitude ( $\lesssim 5\%$ ) as the corrections to the unpolarized cross sections. For unpolarized scattering, this yields a large correction to the extracted value of  $G_E$  at large  $Q^2$ , where the total contribution from  $G_E$  is also small. The polarization measurements are directly sensitive to the ratio  $\mu_p G_E/G_M$ , and so the TPE corrections to this ratio will be of the same magnitude as the correction to the cross section; the large magnification of the effect observed in the Rosenbluth separations does not occur for polarization measurements.

Both the hadronic [22] and partonic [21] approaches can be used to estimate the TPE corrections to the recoil polarization measurements. While the calculations are not strictly valid in the same kinematical regimes, both predict the corrections to be extremely small,  $\lesssim 1\%$ , except for large  $Q^2$  and low  $\varepsilon$  values. The corrections to the existing data are less than 2% for all settings except for the largest  $Q^2$  point, where the corrections are of order 5%, which is still much smaller than the statistical uncertainty of the measurement. However, the sign of the correction is different in the two approaches. As the sign of this correction is not known empirically, and all indications are that it is very small compared to the experimental uncertainties, we do not apply a TPE correction to the polarization measurements. An experiment [56] at Jefferson Lab will map out the  $\varepsilon$  dependence of the polarization transfer at fixed  $Q^2$ , which will provide the first direct information on the TPE correction to polarization transfer.

### III. GLOBAL ANALYSIS

In this section we perform a combined analysis of cross section and polarization data, including both the standard radiative corrections *and* the TPE contributions described above. In Ref. [57], the form factors were ex-

tracted after applying Coulomb distortion corrections applied, but only cross section data were included, and the analysis was limited to very low  $Q^2$  values. This is the first global analysis of form factors in which TPE effects are included in a consistent way from the outset. We apply the TPE corrections to the data, and repeat the global analysis of Ref. [39], with a few important modifications:

- We include additional low  $Q^2$  cross section data [58, 59, 60], more recent cross section results [35, 61], and the full set of polarization transfer and beam-target asymmetry measurements [6, 7, 8, 62, 63, 64, 65, 66, 67, 68].
- We use the TPE calculation from Blunden et al. [22], rather than the phenomenological correction used in Ref. [39]. At high  $Q^2$  (above 1 GeV<sup>2</sup>) we supplement this with an additional TPE correction (Eq. (10)), with a 100% uncertainty, to estimate the contributions from the high mass intermediate states and related (conservative) uncertainties.
- We use a different fitting function, based on Ref. [9], and include high- $Q^2$  constraint points in the fit. The goal is to have a fit valid at both very low  $Q^2$  and the highest  $Q^2$  values of the existing data, with a sensible extrapolation to higher  $Q^2$  values.

In addition to extracting parameterizations of  $G_E$  and  $G_M$  from the global fit, we also take the corrected cross section data in small  $Q^2$  bins, and perform direct LT separations. This allows a test of the consistency between the TPE-corrected cross section results and the polarization measurements. Using the same  $Q^2$  bins we also perform a combined fit to the  $\varepsilon$  dependence of the cross sections and the polarization data, to extract both values and uncertainties for  $G_E$  and  $G_M$ .

Finally, we provide a parameterization of the TPE-*uncorrected* cross section measurements. This parameterization is nearly identical to taking the TPE-corrected form factors and applying the TPE calculation used here, but does not require an explicit calculation of the TPE effects.

### A. Global fitting procedure and results

The combined analysis uses the same general approach outlined in Refs. [17, 39]. As in the previous analyses, we remove the small angle data from Ref. [5], and apply updated radiative correction factors for lepton loop diagrams to some of the older experiments which did not include these corrections. In Ref. [35] a high precision measurement of the elastic cross section was aimed specifically at the ratio  $\mu_p G_E/G_M$ . Their quoted systematic uncertainty is separated into three components: normalization, point-to-point, and a linear  $\varepsilon$  dependent

correction which impacts  $\mu_p G_E/G_M$ , but not does yield random fluctuations or nonlinearity relative to the linear fit. We use only normalization and point-to-point uncertainties, and to include this data in the fit we increased the point-to-point systematic uncertainty from 0.45% to 0.5–0.55% (depending on  $Q^2$ ) such that the uncertainty on  $\mu_p G_E/G_M$  using the inflated point-to-point uncertainty matched the uncertainty as extracted in the more detailed analysis.

After applying the TPE correction to the raw cross sections, we perform a global fit to all of the cross section, polarization transfer, and beam-target asymmetry measurements using the form:

$$G_E, G_M/\mu_p = \frac{1 + \sum_{i=1}^n a_i \tau^i}{1 + \sum_{i=1}^{n+2} b_i \tau^i}. \quad (11)$$

We take  $n = 3$ , which yields 8 fit parameters for each form factor, along with a normalization factor for each independent set of cross section measurements. The fit includes 569 cross section and 54 polarization transfer data points, and yields a reduced  $\chi^2$  of 0.770. Taking  $n = 2$  yields similar fits, with a reduced  $\chi^2$  of 0.802, and changes that are below the uncertainties in the form factors;  $G_M$  changes by  $\lesssim 1\%$  up to  $Q^2 = 10$  GeV<sup>2</sup>,  $G_E$  by less than 3% up to  $Q^2 = 5$  GeV<sup>2</sup>. The normalization factors are consistent between the  $n = 2$  and  $n = 3$  fits, with an RMS variation below 0.2%. The polarization transfer data yield a contribution to  $\chi^2$  of 52 for the 54 data points, indicating good consistency with the cross section data. The parameters from the combined fit are given in Table I, and shown as solid lines in Fig. 3. The parameterization is valid up to at least  $Q^2 = 6$  GeV<sup>2</sup> for  $G_E$ , and  $Q^2 = 30$  GeV<sup>2</sup> for  $G_M$ .

TABLE I: Fit parameters for the extracted proton electric and magnetic form factors, using the parametrization of Eq. (11).

Parameter	$G_M/\mu_p$	$G_E$
$a_1$	-1.465	3.439
$a_2$	1.260	-1.602
$a_3$	0.262	0.068
$b_1$	9.627	15.055
$b_2$	0.000	48.061
$b_3$	0.000	99.304
$b_4$	11.179	0.012
$b_5$	13.245	8.650

The fit function in Eq. (11) is chosen as it gives reasonable behavior in both the limits of low  $Q^2$  and high  $Q^2$ . We constrained the parameters in the denominator ( $b_i$  in Eq. (11)) to be positive, to avoid fits where both the numerator and denominator pass through zero at the same  $Q^2$ , yielding narrow divergences in the fit. Finally, extra high  $Q^2$  “data” points were added to the fit to prevent uncontrolled behavior in the large  $Q^2$  limit. The

high  $Q^2$  constraint points were  $G_M = 0.7 G_D$ , where  $G_D = (1 + Q^2/0.71 \text{ GeV}^2)^{-2}$  is the dipole form factor, at  $Q^2 = 50, 100, 200$ , and  $400 \text{ GeV}^2$ , and at  $G_E = 0$  at  $Q^2 = 10, 15, 20$ , and  $25 \text{ GeV}^2$ . In both cases, the uncertainties were taken to be 50%, 100%, 150%, and 200% of  $G_D$ . This has a negligible effect in the range of the data, but prevents “extreme” behavior in the region where the data do not provide a meaningful separation between  $G_E$  and  $G_M$ .

## B. Rosenbluth analysis

The combined analysis yields a fit for  $G_E$  and  $G_M$ , as well as normalization factors for the various cross section measurements. However, it does not give a clear indication of the consistency between the cross section and polarization data. In this section, we use the normalization factors from the combined global fit to normalize the individual cross section data sets, and perform a global analysis using only the cross section data binned in  $Q^2$ . The results from the TPE-corrected cross section analysis can then be compared directly to the PT measurements, to see to what extent the TPE corrections resolve the discrepancy.

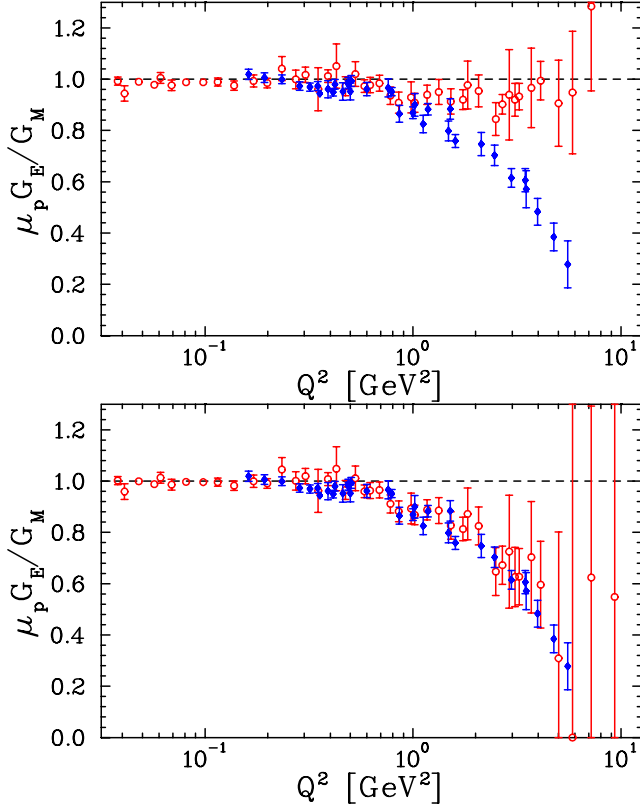


FIG. 2: (Color Online) Ratio  $\mu_p G_E / G_M$  extracted from polarization transfer (filled diamonds) and LT measurements (open circles). The top (bottom) figure shows LT separations without (with) TPE corrections applied to the cross sections.

We begin by taking cross section data in small  $Q^2$  bins and interpolating each cross section to the mean  $Q^2$  value using the fit from Tab. I. The cross section is known well enough that the uncertainty associated with the interpolation is small. The bin size is chosen to keep the interpolation correction small, typically at the 1% level, and an additional uncertainty equal to 3% of the correction is applied to the corrected point. We then perform an LT separation to extract  $G_E / G_M$ . We determine a systematic uncertainty associated with the scale factors by taking each data set and varying its normalization by the estimated scale uncertainty. Note that because we have used the global fit to estimate the normalization factors, we have a smaller scale uncertainty than quoted for the individual measurements. We take the scale uncertainty after the global fit to be the smaller of 1% or half of the originally quoted normalization uncertainty. For the analysis including TPE corrections, we also take the additional TPE correction arising from the high mass intermediate states and vary it by  $\pm 100\%$  to estimate the additional TPE uncertainty for large  $Q^2$ .

In Fig. 2 we show a comparison of the PT data (filled diamonds) and the LT separation data (open circles). The data sets are completely independent, except for the use of the normalization factors from the global fit of Sec. III A. The top panel shows the global LT analysis without applying TPE corrections, while the bottom is with TPE corrections. The uncertainties in the LT separation increase significantly at large  $Q^2$  values when the TPE corrections are applied. This is in part due to the uncertainty assigned to the high  $Q^2$  TPE corrections, but mainly due to the fact that the LT separation is a measure of  $(G_E / G_M)^2$  rather than  $G_E / G_M$ , so a reduction in the slope yields a constant absolute uncertainty in  $(G_E / G_M)^2$ , which maps into a larger absolute uncertainty in  $G_E / G_M$ .

Note that for very low  $Q^2$ , the TPE correction does not go to zero. In fact, the correction to the unpolarized cross section becomes zero for  $Q^2 \approx 0.3 \text{ GeV}^2$ , and changes sign for lower  $Q^2$  values. This appears to be a largely model-independent result, which persists even for the case of point-like nucleons. Thus, even the extremely low  $Q^2$  extractions are modified by TPE. With the TPE correction applied, the average value of  $\mu_p G_E / G_M$  for  $Q^2 < 0.2 \text{ GeV}^2$  goes from 0.988(4) to 0.997(4), showing that  $G_E$  and  $G_M$  have consistent low- $Q^2$  behavior.

One of the unique features of the TPE correction is that it introduces nonlinearity in the  $\varepsilon$  dependence of the cross section. Although part of the TPE contribution is linear in  $\varepsilon$ , observation of nonlinearity in the data would provide direct evidence of TPE effects in elastic scattering. To quantify the amount of nonlinearity in the data, we fit the reduced cross section to a quadratic in  $\varepsilon$ , as in Ref. [47]:

$$\sigma_R = P_0[1 + P_1(\varepsilon - 0.5) + P_2(\varepsilon - 0.5)^2], \quad (12)$$

where  $P_2$  represents the fractional  $\varepsilon$ -curvature parameter, relative to the average ( $\varepsilon = 0.5$ ) reduced cross sec-



tion. With the inclusion of TPE corrections, the average nonlinearity parameter,  $\langle P_2 \rangle$ , is found to increase from  $1.9 \pm 2.7\%$  to  $4.3 \pm 2.8\%$ . While the extracted nonlinearity increases with the TPE corrections, it is not large enough to be considered inconsistent with  $P_2 = 0$ . In addition, the results from Ref. [47] are dominated by higher  $Q^2$  points, where we do not include nonlinearities in the TPE contributions from higher mass intermediate states. Including the single-experiment LT separations from the new low  $Q^2$  data sets used in this analysis, we find  $\langle P_2 \rangle = 2.8 \pm 2.4\%$  (after TPE), again consistent with no nonlinearities.

### C. Extraction of $G_E$ and $G_M$ from global analysis

In this section we extract individual  $G_E$  and  $G_M$  points and uncertainties over the full  $Q^2$  range where the form factors can be separated. The analysis follows that of the corrected cross section data in the previous section, but now we include the PT measurements in each  $Q^2$  bin as part of the fit. The results for  $Q^2 < 6 \text{ GeV}^2$ , where  $G_E$  and  $G_M$  can be separated, are given in Table II, and shown in Fig. 3.

For the combined fit, we fit  $G_E$  and  $G_M$  to the combination of cross section and polarization transfer data in each small  $Q^2$  bin. For the cross sections, we use the TPE-corrected cross section measurements, and normalize each data set using the scale factors found in the global fit (Sec. III A). After making the initial fit for  $G_E$  and  $G_M$ , we scale each data set by the estimated normalization uncertainty (as in Sec. III B) to determine its contribution to the systematic uncertainty, and add these in quadrature to determine the total uncertainty in  $G_E$ ,  $G_M$  and the ratio due to the normalization uncertainties.

In addition to improving the overall precision, combining the cross section and PT results has the added benefit of decreasing the correlation in the uncertainties in  $G_E$  and  $G_M$ . The Rosenbluth separation tends to yield a large anti-correlation between the uncertainties for  $G_E$  and  $G_M$ , and thus an enhanced uncertainty on the ratio. The PT data measure the ratio directly, thus dramatically reducing this correlation. Therefore, in Tab. II, we provide values and uncertainties for both the individual form factors and the form factor ratio.

### D. Extraction of $G_M$ at high $Q^2$

In the extraction of  $G_M$  for  $Q^2 > 6 \text{ GeV}^2$ , we do not know the value for  $G_E$ , and thus have to make an assumption to extract  $G_M$ . We extract  $G_M$  under two different assumptions for the ratio of  $G_E/G_M$ . First, we assume that the  $G_E$  term is negligible above  $6 \text{ GeV}^2$ , which would be the case if  $G_E$  approaches zero and then stays small. Second, we assume a linear falloff,  $\mu_p G_E/G_M = 1 - 0.135(Q^2 - 0.24)$ , from Ref. [8]. Up to  $Q^2 \approx 14 \text{ GeV}^2$ , this yields a smaller contribution from

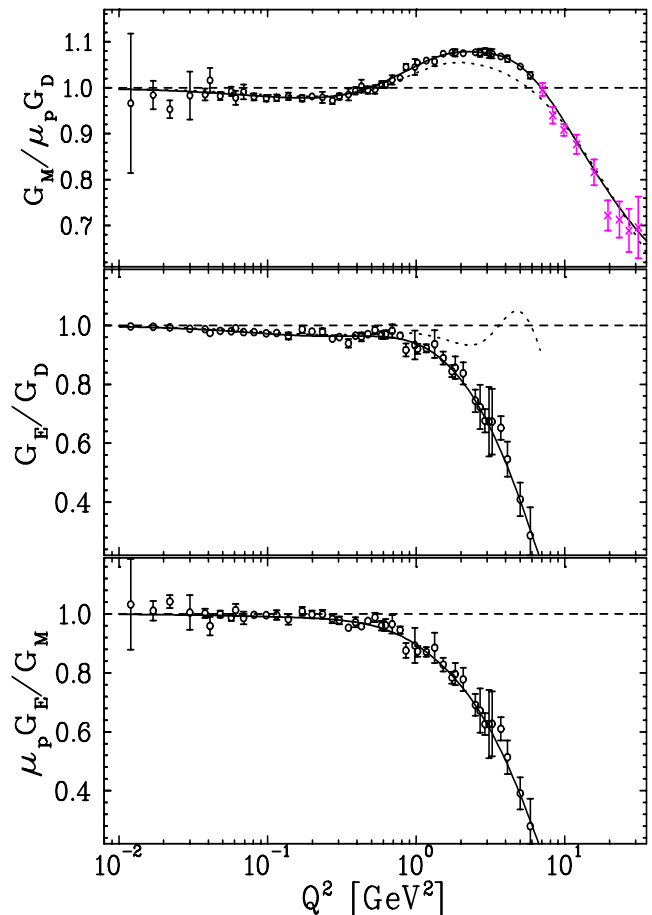


FIG. 3: (Color online) Extracted values of  $G_E$  and  $G_M$  from the global analyses. The open circles are the results of the combined analysis of the cross section data and polarization measurements (Sec. III C, Tab. II). The magenta crosses are the extracted values of  $G_M$  (Tab. III) for the high  $Q^2$  region, where  $G_E$  cannot be extracted. The solid lines are the fits to TPE-corrected cross section and polarization data (Sec. III A). The dotted curves show the results of taking  $G_E$  and  $G_M$  to be  $\sqrt{\sigma_L}$  and  $\sqrt{\sigma_T}$ , respectively, from a fit to the TPE-uncorrected reduced cross section (Appendix A), i.e. the value one would obtain using only cross section data and ignoring TPE.

$G_E$  than was assumed in previous analyses, where it was assumed that  $\mu_p G_E/G_M = 1$ . At higher  $Q^2$ , this fit yields  $|\mu_p G_E/G_M| > 1$ , and thus a *larger*  $G_E$  contribution, almost 10 times what was assumed in the initial analysis of the Sill data [69] at  $Q^2 = 30 \text{ GeV}^2$ . This yields a significant change in the  $Q^2$  dependence of the reduced cross section. Instead of the electric contribution decreasing from 6% almost to zero as one went from 5 to  $30 \text{ GeV}^2$ , the linear decrease in  $G_E$  implies almost no contribution at  $5\text{--}9 \text{ GeV}^2$ , and maximum contribution of  $\approx 6\%$  at the highest  $Q^2$ .

The final quoted values for  $G_M$  are taken as the average of the values obtained assuming  $\mu_p G_E/G_M = 0$ , and  $\mu_p G_E/G_M = 1 - 0.135(Q^2 - 0.24)$ , with half of the



difference taken as the associated uncertainty. Note that the additional TPE component meant to estimate the high mass intermediate state contributions, as discussed in Sec. II C, yields a significant correction (and uncertainty) of 3–4.5% to the cross section over the range of the high  $Q^2$  data. Table III shows the extracted value of  $G_M$  based on the above assumptions, along with the value of  $G_E$  needed to reproduce the TPE-corrected cross sections when combined with the quoted values of  $G_M$ . Because we average the extracted  $G_M$  values, and the cross section correction due to  $G_E$  depends on  $G_E^2$ , this corresponds to taking the average value of  $G_E^2$  rather than the average  $G_E$ . Above  $Q^2=10$  GeV<sup>2</sup>, the only data included is from Sill, *et al.* [69]. There is also data from an earlier SLAC experiment [70], but both the scale and statistical uncertainties are much larger than for the later measurements, and so this data is not included.

#### IV. CONCLUSION

We have performed the first global analysis of elastic electron–proton scattering data taking into account two-photon exchange contributions and their associated uncertainties. The analysis combines the corrected Rosenbluth cross section and polarization transfer data, and the corrected form factors  $G_E$  and  $G_M$  have been extracted over the full range of  $Q^2$  of existing data, up to  $Q^2 \approx 6$  GeV<sup>2</sup> and  $G_E$  and  $Q^2 \approx 30$  GeV<sup>2</sup> for  $G_M$ .

The applied TPE corrections are based on the hadronic model of Ref. [22] for the nucleon elastic intermediate state, but with improved input form factors at the internal vertices. These have been supplemented by inelastic contributions estimated from recent calculations with explicit excited  $N^*$  intermediate states [23, 27, 41], and from GPD-based partonic calculations [20]. The uncertainty in describing the (off-shell) intermediate states is the main source of model dependence in the analysis. This uncertainty is more tractable, and relatively mild, at low  $Q^2$ , but becomes larger at high  $Q^2$  values. For the higher-mass intermediate state contributions, which are more important for the high  $Q^2$  data, we assign a 100% uncertainty on the inelastic TPE correction.

The resulting TPE corrections to  $G_E$  are significant in the region  $2 \lesssim Q^2 \lesssim 6$  GeV<sup>2</sup>, where the LT and PT data are in most striking disagreement, and here they bring the LT data into good agreement with the PT results for  $G_E/G_M$ . The corrections to  $G_M$  are smaller, but can be a few percent at moderately large  $Q^2$  values. We provide a convenient parameterization of the corrected  $G_E$  and  $G_M$  form factors, as well as of the reduced elastic cross section, parameterized by effective form factors which contain TPE effects.

This analysis is based on the assumption that two-photon exchange fully resolves the observed discrepancy in the form factor extractions. While this is supported by recent calculations and provides a consistent explanation of all the measurements, definitive evidence for the role of

TPE in elastic  $ep$  scattering is still lacking. Experiment E04-116 [55], using a beam of  $e^+e^-$  pairs produced from a secondary photon beam at Jefferson Lab, will make simultaneous measurements of  $e^+p$  and  $e^-p$  elastic cross sections up to  $Q^2 \sim 2$  GeV<sup>2</sup>. The  $e^+p/e^-p$  ratio is directly sensitive to TPE effects. A proposal to perform a precise ( $\sim 1\%$ ) comparison of  $e^-p$  and  $e^+p$  scattering at  $Q^2 = 1.6$  GeV<sup>2</sup> and  $\varepsilon \approx 0.4$  has also been made at the VEPP-3 storage ring [54].

Beyond the Born approximation, we also expect nonlinearities in the  $\varepsilon$  dependence of the cross section. With the existing data, the results do not show a significant nonlinearity before or after applying TPE corrections, and so do not yet set significant limits. A recently completed Jefferson Lab experiment [71] will provide an accurate measurement of the  $\varepsilon$  dependence of the elastic  $ep$  cross section, with sufficient sensitivity to test the calculated nonlinearities. Additional upcoming measurements [56, 72] will extend polarization transfer measurements to higher  $Q^2$  values, as well as examining the  $\varepsilon$  dependence of polarization transfer measurements. This increase in  $Q^2$  will allow for a clean extraction of  $G_E$  and improved uncertainties on  $G_M$  up to  $\sim 9$  GeV<sup>2</sup>, while the  $\varepsilon$  dependence will be the first measurement sensitive to TPE in polarization transfer.

On the theoretical front, the largest uncertainty arises from poor knowledge of the contributions to the TPE amplitude from high mass intermediate states, beyond those of the nucleon elastic. This introduces significant model dependence in the correction, especially at large  $Q^2$ . It can be reduced by using phenomenological input for the virtual Compton scattering amplitude at intermediate and high  $Q^2$  values. In future it would be desirable to merge the low  $Q^2$  hadronic calculations with the high  $Q^2$  partonic approach, and develop a framework which enables TPE corrections to be consistently described over the entire  $Q^2$  range of data. The present analysis should at the very least serve to highlight this need. Finally, we may expect in future more information on virtual Compton scattering to come from lattice QCD, although calculation of four-point functions of this type is currently still in its infancy.

#### APPENDIX A: PARAMETERIZATION OF ELASTIC CROSS SECTION

In this appendix we provide a convenient parameterization of elastic cross section. One can use the fits to  $G_E$  and  $G_M$  in Sec. III C to calculate the Born cross section, and then apply radiative corrections, including TPE, to predict the measured cross section. However, this requires an explicit calculation of the TPE correction to the cross section, consistent with the calculation used to correct the cross section measurements. It is useful for some applications to work directly with the elastic cross section, without necessarily requiring knowledge of the fundamental form factors. We therefore provide

a separate parameterization of the elastic cross section and uncertainties *without* TPE corrections applied to the data. This will provide a simple and reliable, model-independent parameterization for the cross section without direct reference to TPE effects.

We parameterize the full elastic reduced cross section (Born + TPE corrections) by:

$$\sigma_R^{\text{elas}} = \tau F_m(Q^2, \varepsilon) + \varepsilon F_e(Q^2, \varepsilon), \quad (\text{A1})$$

where  $F_m$  and  $F_e$  are effective magnetic and electric form factors, respectively, which absorb the effects of multiple photon exchange. In the Born approximation these obviously approach the usual Sachs form factors:

$$F_m(Q^2, \varepsilon) \rightarrow G_M(Q^2), \quad F_e(Q^2, \varepsilon) \rightarrow G_E(Q^2). \quad (\text{A2})$$

In principle, the form factors  $F_e$  and  $F_m$  depend on both  $Q^2$  and  $\varepsilon$ , but as calculations and existing data [47] indicate extremely small deviations from linearity, we can at present safely neglect this additional  $\varepsilon$  dependence,

and use the form from Eq. (11) when fitting  $F_m$  and  $F_e$ . We repeat the global fit described in Sec. III A, using only *uncorrected* cross section data. We keep the normalization constants from the different data sets fixed to the values obtained from the global fit, as these represent our best estimation of the true normalization factors of the cross section measurements. The results of the fit for the cross section in Eq. (A1) in terms of the effective form factors  $F_e$  and  $F_m$  are given in Table IV.

## ACKNOWLEDGMENTS

This work was supported by the U. S. Department of Energy, Office of Nuclear Physics, under contract DE-AC02-06CH11357 and contract DE-AC05-06OR23177 under which Jefferson Science Associates, LLC operates the Thomas Jefferson National Accelerator Facility. We thank S. Kondratyuk for providing the results from Ref. [27].

- 
- [1] C. E. Hyde-Wright and K. de Jager, *Ann. Rev. Nucl. Part. Sci.* **54**, 217 (2004).
  - [2] C. F. Perdrisat, V. Punjabi, and M. Vanderhaeghen (2006), hep-ph/0612014.
  - [3] H. Gao, *Int. J. Mod. Phys. A* **20**, 1595 (2005).
  - [4] J. Arrington, C. D. Roberts, and J. M. Zanotti (2006), nucl-th/0611050.
  - [5] R. C. Walker et al., *Phys. Rev. D* **49**, 5671 (1994).
  - [6] V. Punjabi et al., *Phys. Rev. C* **71**, 055202 (2005).
  - [7] O. Gayou et al., *Phys. Rev. C* **64**, 038202 (2001).
  - [8] O. Gayou et al., *Phys. Rev. Lett.* **88**, 092301 (2002).
  - [9] J. J. Kelly, *Phys. Rev. C* **66**, 065203 (2002).
  - [10] D. H. Lu, S. N. Yang, and A. W. Thomas, *J. Phys. G* **26**, L75 (2000), nucl-th/9911065.
  - [11] A. J. Buchmann and E. M. Henley, *Phys. Rev. C* **63**, 015202 (2001), hep-ph/0101027.
  - [12] G. A. Miller, *Phys. Rev. C* **68**, 022201 (2003), nucl-th/0304076.
  - [13] H. H. Matevosyan, A. W. Thomas, and G. A. Miller, *Phys. Rev. D* **72**, 065204 (2005), nucl-th/0508049.
  - [14] F. Gross, G. Ramalho, and M. T. Pena (2006), nucl-th/0606029.
  - [15] A. Kvinikhidze and G. A. Miller, *Phys. Rev. C* **73**, 065203 (2006), nucl-th/0603035.
  - [16] P. Wang, D. B. Leinweber, A. W. Thomas, and R. D. Young, *Phys. Rev. D* **75**, 073012 (2007), hep-ph/0701082.
  - [17] J. Arrington, *Phys. Rev. C* **68**, 034325 (2003).
  - [18] P. A. M. Guichon and M. Vanderhaeghen, *Phys. Rev. Lett.* **91**, 142303 (2003).
  - [19] P. G. Blunden, W. Melnitchouk, and J. A. Tjon, *Phys. Rev. Lett.* **91**, 142304 (2003).
  - [20] Y. C. Chen, A. Afanasev, S. J. Brodsky, C. E. Carlson, and M. Vanderhaeghen, *Phys. Rev. Lett.* **93**, 122301 (2004).
  - [21] A. V. Afanasev, S. J. Brodsky, C. E. Carlson, Y.-C. Chen, and M. Vanderhaeghen, *Phys. Rev. D* **72**, 013008 (2005).
  - [22] P. G. Blunden, W. Melnitchouk, and J. A. Tjon, *Phys. Rev. C* **72**, 034612 (2005).
  - [23] S. Kondratyuk, P. G. Blunden, W. Melnitchouk, and J. A. Tjon, *Phys. Rev. Lett.* **95**, 172503 (2005).
  - [24] P. Jain, S. D. Joglekar, and S. Mitra (2006), hep-ph/0606149.
  - [25] D. Borisyuk and A. Kobushkin (2006), nucl-th/0606030.
  - [26] C. E. Carlson and M. Vanderhaeghen (2007), hep-ph/0701272.
  - [27] S. Kondratyuk and P. G. Blunden, *Phys. Rev. C* **75**, 038201 (2007), nucl-th/0701003.
  - [28] A. I. Akhiezer and M. P. Rekalo, *Sov. J. Part. Nucl.* **4**, 277 (1974).
  - [29] N. Dombey, *Rev. Mod. Phys.* **41**, 236 (1969).
  - [30] M. J. Alguard et al., *Phys. Rev. Lett.* **37**, 1258 (1976).
  - [31] T. W. Donnelly and A. S. Raskin, *Annals Phys.* **169**, 247 (1986).
  - [32] L. W. Mo and Y.-S. Tsai, *Rev. Mod. Phys.* **41**, 205 (1969).
  - [33] L. C. Maximon and J. A. Tjon, *Phys. Rev. C* **62**, 054320 (2000).
  - [34] A. V. Afanasev, *Phys. Lett. B* **514**, 369 (2001).
  - [35] I. A. Qattan et al., *Phys. Rev. Lett.* **94**, 142301 (2005).
  - [36] Y. S. Tsai, *Tech. Rep.*, SLAC Report (1971).
  - [37] R. Ent et al., *Phys. Rev. C* **64**, 054610 (2001).
  - [38] P. Mergell, U. G. Meissner, and D. Drechsel, *Nucl. Phys. A* **596**, 367 (1996), hep-ph/9506375.
  - [39] J. Arrington, *Phys. Rev. C* **69**, 022201(R) (2004).
  - [40] E. J. Brash, A. Kozlov, S. Li, and G. M. Huber, *Phys. Rev. C* **65**, 051001(R) (2002).
  - [41] J. Tjon and W. Melnitchouk, in preparation.
  - [42] S. D. Drell and M. Ruderman, *Phys. Rev.* **106**, 561 (1957).
  - [43] S. D. Drell and S. Fubini, *Phys. Rev.* **113**, 741 (1959).
  - [44] G. K. Greenhut, *Phys. Rev.* **184**, 1860 (1969).
  - [45] S. Kondratyuk and O. Scholten, *Phys. Rev. C* **64**, 024005 (2001), nucl-th/0103006.
  - [46] W. Melnitchouk, R. Ent, and C. Keppel, *Phys. Rept.*

- 406**, 127 (2005).
- [47] V. Tvaskis et al., Phys. Rev. C **73**, 025206 (2006).
  - [48] A. Browman, F. Liu, and C. Schaerf, Phys. Rev. **139**, B1079 (1965).
  - [49] J. Mar et al., Phys. Rev. Lett. **21**, 482 (1968).
  - [50] R. L. Anderson, B. Borgia, G. L. Cassiday, J. W. DeWire, A. S. Ito, and E. C. Loh, Phys. Rev. Lett. **17**, 407 (1966).
  - [51] W. Bartel, B. Dudelzak, H. Krehbiel, J. M. McElroy, R. J. Morrison, W. Schmidt, V. Walther, and G. Weber, Phys. Lett. B **25**, 242 (1967).
  - [52] B. Bouquet, D. Benaksas, B. Grossetete, B. Jean-Marie, G. Parrou, J. P. Poux, and R. Tchapoutian, Phys. Lett. B **26**, 178 (1968).
  - [53] J. Arrington, Phys. Rev. C **69**, 032201(R) (2004).
  - [54] J. Arrington, D. M. Nikolenko, et al., Proposal for positron measurement at VEPP-3, nucl-ex/0408020.
  - [55] W. Brooks, A. Afanasev, J. Arrington, K. Joo, B. Raue, L. Weinstein, et al., Jefferson Lab experiment E04-116.
  - [56] R. Gilman, L. Pentchev, C. Perdrisat, R. Suleiman, et al., Jefferson Lab experiment E04-019.
  - [57] J. Arrington and I. Sick (2006), nucl-th/0612079.
  - [58] D. Frerejacque, D. Benaksas, and D. J. Drickey, Phys. Rev. **141**, 1308 (1966).
  - [59] D. Ganichot, B. Grossetete, and D. B. Isabelle, Nucl. Phys. **A178**, 545 (1972).
  - [60] B. Dudelzak, Ph.D. thesis, University of Parix (1965).
  - [61] M. E. Christy et al., Phys. Rev. C **70**, 015206 (2004).
  - [62] B. D. Milbrath et al., Phys. Rev. Lett. **82**, 2221(E) (1999).
  - [63] T. Pospischil et al. (A1 Collaboration), Eur. Phys. J. **A12**, 125 (2001).
  - [64] S. Strauch et al. (Jefferson Lab E93-049), Phys. Rev. Lett. **91**, 052301 (2003).
  - [65] G. MacLachlan et al., Nucl. Phys. **A764**, 261 (2006).
  - [66] M. K. Jones et al. (Resonance Spin Structure), Phys. Rev. C **74**, 035201 (2006).
  - [67] C. B. Crawford et al., Phys. Rev. Lett. **98**, 052301 (2007).
  - [68] G. Ron et al. (2007), arXiv:0706.0128 [nucl-ex].
  - [69] A. F. Sill et al., Phys. Rev. D **48**, 29 (1993).
  - [70] D. H. Coward et al., Phys. Rev. Lett. **20**, 292 (1968).
  - [71] J. Arrington et al., Jefferson Lab experiment E05-017.
  - [72] C. F. Perdrisat, V. Punjabi, M. K. Jones, E. Brash, et al., Jefferson Lab experiment E04-108.

TABLE II: Extracted values for the corrected form factors, relative to the dipole form:  $G_D = (1 + Q^2/0.71)^{-2}$ .

$Q^2[\text{GeV}^2]$	$G_E/G_D$	$G_M/(\mu_p G_D)$	$\mu_p G_E/G_M$
0.007	1.000±0.006	0.715±0.393	1.400±0.712
0.012	0.996±0.006	0.966±0.152	1.032±0.154
0.017	0.995±0.003	0.984±0.031	1.011±0.033
0.022	0.993±0.003	0.953±0.019	1.042±0.022
0.030	0.988±0.007	0.983±0.052	1.005±0.059
0.038	0.987±0.004	0.985±0.013	1.002±0.016
0.041	0.974±0.007	1.016±0.027	0.959±0.031
0.048	0.981±0.005	0.982±0.009	0.999±0.012
0.057	0.980±0.005	0.992±0.010	0.988±0.012
0.061	0.990±0.008	0.978±0.015	1.013±0.021
0.069	0.977±0.007	0.991±0.016	0.986±0.021
0.081	0.977±0.005	0.980±0.008	0.997±0.011
0.098	0.973±0.007	0.977±0.007	0.996±0.010
0.115	0.974±0.011	0.978±0.007	0.996±0.016
0.138	0.964±0.012	0.981±0.008	0.982±0.018
0.171	0.986±0.012	0.977±0.007	1.009±0.015
0.199	0.979±0.011	0.981±0.006	0.998±0.013
0.234	0.978±0.012	0.979±0.012	0.999±0.015
0.273	0.955±0.010	0.972±0.008	0.983±0.014
0.304	0.960±0.010	0.981±0.007	0.978±0.013
0.350	0.939±0.014	0.985±0.013	0.953±0.009
0.390	0.965±0.011	0.993±0.008	0.972±0.017
0.428	0.961±0.015	1.003±0.014	0.958±0.010
0.473	0.970±0.011	0.995±0.008	0.976±0.011
0.528	0.984±0.013	0.996±0.009	0.988±0.016
0.584	0.967±0.013	1.007±0.007	0.960±0.016
0.622	0.969±0.014	1.007±0.007	0.962±0.020
0.689	0.981±0.023	1.017±0.010	0.965±0.031
0.779	0.965±0.011	1.021±0.005	0.945±0.013
0.853	0.916±0.022	1.045±0.007	0.876±0.025
0.979	0.933±0.049	1.045±0.017	0.893±0.060
1.020	0.920±0.017	1.054±0.006	0.873±0.018
1.170	0.922±0.014	1.059±0.005	0.871±0.016
1.330	0.936±0.047	1.057±0.010	0.885±0.051
1.520	0.889±0.022	1.074±0.006	0.828±0.023
1.740	0.844±0.020	1.077±0.004	0.784±0.020
1.830	0.856±0.038	1.076±0.008	0.796±0.038
2.070	0.837±0.038	1.075±0.006	0.778±0.039
2.500	0.744±0.038	1.077±0.005	0.691±0.037
2.690	0.723±0.075	1.076±0.009	0.672±0.075
2.900	0.676±0.039	1.079±0.007	0.626±0.037
3.090	0.673±0.118	1.075±0.010	0.626±0.116
3.240	0.673±0.112	1.074±0.010	0.627±0.110
3.710	0.652±0.040	1.068±0.005	0.610±0.039
4.110	0.546±0.059	1.063±0.007	0.514±0.057
5.010	0.409±0.057	1.046±0.005	0.391±0.055
5.850	0.287±0.095	1.027±0.007	0.280±0.093

TABLE III: Extracted values for the high  $Q^2$   $G_M$  results, along with the  $G_E$  values assumed in the extraction.

$Q^2[\text{GeV}^2]$	$G_M/(\mu_p G_D)$	$G_E/G_D$
7.081	$0.996 \pm 0.014$	+0.054
8.294	$0.940 \pm 0.018$	-0.058
9.848	$0.908 \pm 0.013$	-0.191
11.990	$0.877 \pm 0.021$	-0.364
15.720	$0.816 \pm 0.028$	-0.629
19.470	$0.721 \pm 0.033$	-0.814
23.240	$0.713 \pm 0.039$	-1.062
26.990	$0.689 \pm 0.047$	-1.273
31.200	$0.696 \pm 0.067$	-1.564

TABLE IV: Parameters for the fit to the TPE-*uncorrected* cross section of Eq. (A2), using the parameterization of Eq. (11) for  $F_m$  and  $F_e$ .

Parameter	$F_m/\mu_p$	$F_e$
$a_1$	-2.151	-1.651
$a_2$	4.261	1.287
$a_3$	0.159	-0.185
$b_1$	8.647	9.531
$b_2$	0.001	0.591
$b_3$	5.245	0.000
$b_4$	82.817	0.000
$b_5$	14.191	4.994